

# The Ultra Luminous X-ray sources in the High Velocity System of NGC 1275

O. González-Martín<sup>1,2\*</sup>, A.C. Fabian<sup>2</sup> and J.S. Sanders<sup>2</sup>

<sup>1</sup>*Instituto de Astrofísica de Andalucía (CSIC), Apdo 3004, 18080 Granada, Spain*

<sup>2</sup>*Institute of Astronomy, Madingley Road, Cambridge CB3 0HA*

19 September 2018

## ABSTRACT

We report the results of a study of X-ray point sources coincident with the High Velocity System (HVS) projected in front of NGC 1275. A very deep X-ray image of the core of the Perseus cluster made with the *Chandra Observatory* has been used. We find a population of Ultra-Luminous X-ray sources (ULX; 7 sources with  $L_X(0.5 - 7.0\text{keV}) > 7 \times 10^{39} \text{erg s}^{-1}$ ). As with the ULX populations in the Antennae and Cartwheel galaxies, those in the HVS are associated with a region of very active star formation. Several sources have possible optical counterparts found on *HST* images, although the X-ray brightest one does not. Absorbed power-law models fit the X-ray spectra, with most having a photon index between 2 and 3.

**Key words:** galaxies: clusters: individual: Perseus - ULX - galaxies: individual: NGC 1275

## 1 INTRODUCTION

The study of Ultra-Luminous X-ray sources (ULX) has been greatly expanded by the high spatial resolution and spectral grasp of the *Chandra* and *XMM-Newton* observatories, respectively. ULX sources (Fabbiano & White 2003; Miller & Colbert 2004) have 2–10 keV X-ray luminosities exceeding  $10^{39} \text{erg s}^{-1}$  and are found some distance from the centres of galaxies; they are not active galactic nuclei. Their luminosity exceeds that for a  $10 M_\odot$  black hole accreting at the Eddington limit which radiates isotropically and so have created much interest in the possibility that they contain even higher mass black holes, such as Intermediate Black Holes (IMBH) of  $\sim 10^3 M_\odot$  (Makishima et al 2000; Miller, Fabian & Miller 2004). Alternatively they may appear so luminous because of beaming (Reynolds et al 1999; King et al 2001, Zezas & Fabbiano 2002) or due to super Eddington accretion (Begelman 2002).

ULX are most common in starburst galaxies and in very active star-forming regions, such as in the Antennae and the Cartwheel galaxy, where populations of tens of them are found (Zezas et al 2002; Gao et al 2003; Wolter & Trinchieri 2004). In some cases variability rules out the possibility that they are just clusters of lower-luminosity objects. The origin of IMBH is unclear. They may form as a result of binary interactions in dense stellar environments (Portegies Zwart & McMillan 2002). A comparison of IMBH ULX candidates with a number of well known stellar-mass black holes candidates (BHC; Miller et al 2004) demonstrates that the ULX are more luminous but have cooler thermal disk components than standard stellar-mass BHC. Therefore, ULX in this sample are clearly

different from the sample of stellar-mass BHC and are consistent with being IMBH.

Here we report on the discovery of a population of 8 point X-ray sources to the N of the nucleus of NGC 1275, which is the central galaxy in the Perseus cluster. All exceed  $10^{39} \text{erg s}^{-1}$  in X-ray luminosity, and 7 are formally ULX, if they are at the distance of the cluster. The spatial region where they lie coincides with the High Velocity System of NGC 1275. We assume that they are part of that system. We see no other point sources (apart from the nucleus) over the body of NGC 1275 (Fig. 1).

NGC 1275 is embedded in a complex multiphase environment. Optical imaging and spectroscopy first established the existence of two distinct emission-line system toward NGC 1275: a low-velocity component associated with the galaxy itself at  $5200 \text{km s}^{-1}$  and a high-velocity component at  $8200 \text{km s}^{-1}$  projected nearby on the sky (Minkowski 1955, 1957). This latter component is associated with a small gas-rich galaxy falling into the cluster along our line of sight (Haschick, Crane & van der Hulst 1982). A merger scenario has been proposed (Minkowski 1955, 1957). However, interaction of the low and/or high-velocity system with a third gas-rich galaxy or system of galaxies (Holtzman et al. 1992; Conselice, Gallagher & Wyse 2001), or influences from the surrounding dense intracluster medium (ICM) (Sarazin 1988; Boroson 1990; Caulet et al. 1992) have been discussed.

Deep *Chandra* observations have clarified the position of the High Velocity System (HVS). The depth of the observed X-ray absorption (e.g. Fig. 1) is not filled by emission from hot gas projected along the line-of-sight so the HVS must lie well in front of NGC 1275. Gillmon, Sanders & Fabian (2004) have estimated a lower limit on the distance of the HVS from the nucleus of 57 kpc. The low- and high-velocity system are therefore not yet directly in-

\* E-mail: omaira@iaa.es

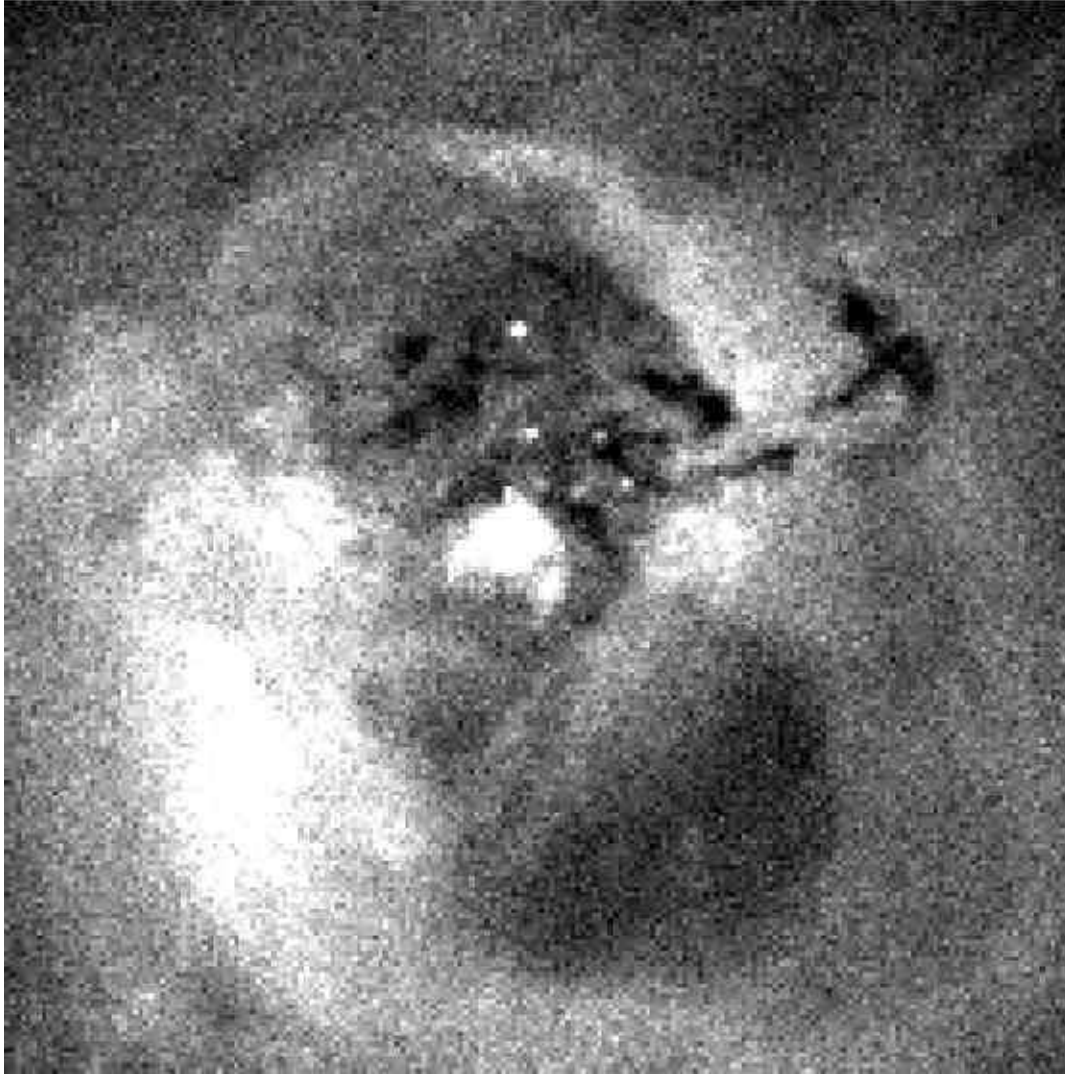


**Figure 1.** NGC 1275 in the 0.3–7.0 keV band. Pixels are 0.49 arcsec in size and the N-S height of the image is 97 arcsec. North is to the top and east is to the left in this image. The point sources which we identify as ULX are located in the high-velocity system is seen in absorption to the north of the bright nucleus. None are seen in the south lobe

teracting. The HVS is however strongly interacting with the ICM of the Perseus cluster, which has triggered strong star formation. In this paper we describe the detailed analysis of the X-ray spatial and spectral properties of the discrete sources in the high velocity system.

The paper is organized as follows: in Sect. 2 and 3 we present reduction and results from the imaging analysis and spectral analysis, respectively; in Sect. 4 we discuss the results; and Sect. 5 summarizes our findings.

Throughout this paper we use a redshift of 0.018 and  $H_0 = 70 \text{ km s}^{-1} \text{ Mpc}^{-1}$ . This gives a luminosity distance to the cluster of 80 Mpc; 1 arcsec corresponds to a physical distance of 370 pc.

## 2 IMAGING ANALYSIS

The *Chandra* datasets included in this analysis are listed in Table 1. The total exposure time, after removing periods containing flares, is 890 ks. To prepare the data for analysis, all of the datasets were reprocessed to use the latest appropriate gain file (acisD2000-01-

29gain.ctiN0003). The datasets analysed each used an aimpoint on the ACIS-S3 CCD. The datasets were filtered using the lightcurve in the 2.5 to 7 keV band on ACIS-S1 CCD, which is a back-illuminated CCD like the ACIS-S3. The CIAO `LC_CLEAN` tool was used to remove periods 20 per cent away from the median count rate for all the lightcurves. This procedure was not used for datasets 03209 and 04289 which did not include the S1 CCD, however no flares were seen in these observations on the S3 CCD. Each of the observations was reprojected to match the coordinate system of the 04952 observation.

The 900 ks X-ray image covering the energy range 0.3–0.8 keV is shown in Fig 2. The bright NGC 1275 nucleus is clearly seen at RA  $3^h 19^m 48^s$  and Dec.  $+41^\circ 30' 42''$  (J2000) and the high-velocity system is seen in absorption to the north of the nucleus.

The CIAO `CELLDETECT` source detection routine was then used on the reprocessed level 2 event data to produce a preliminary list of point sources. The cell size ranges between 4 pixels to 8 pixels. This algorithm strongly depends on the local background and the detection cell is not adjustable to the size of the source.

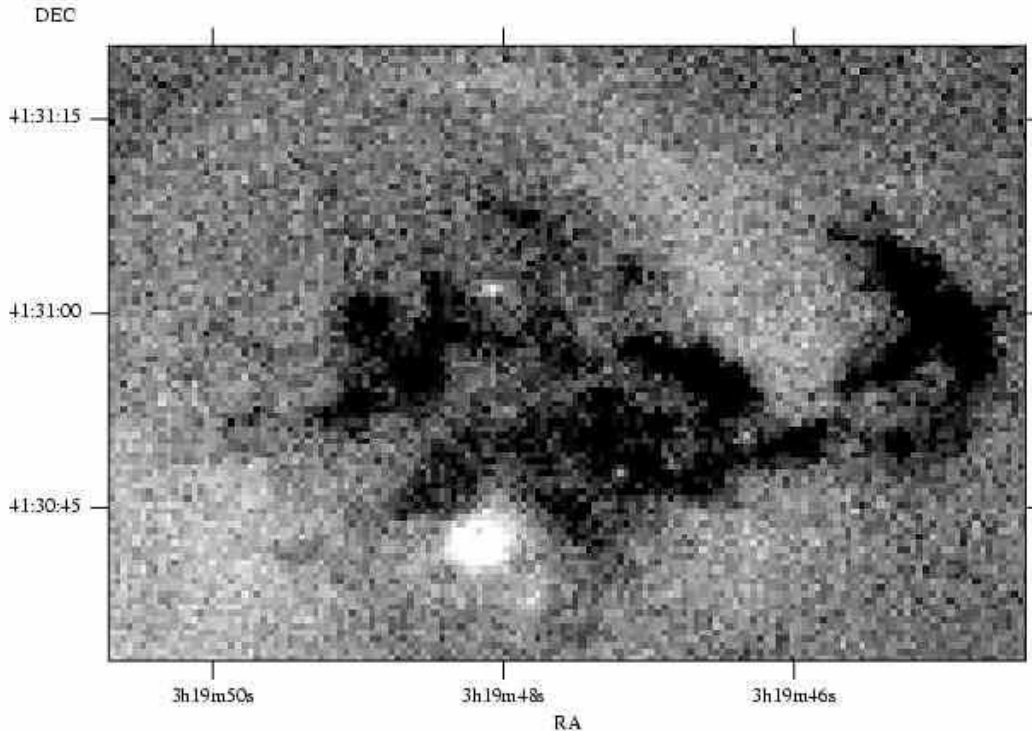


**Figure 2.** The central region of NGC 1275 in the 0.3–0.8 keV band. Pixels are 0.49 arcsec in dimension and the entire image is  $1.77 \times 0.89$  arcmin<sup>2</sup>. North is to the top and east is to the left in this image. The high-velocity system is seen in absorption to the north of the bright nucleus which is at RA  $3^{\text{h}}19^{\text{m}}48^{\text{s}}$ , Dec.  $+41^{\circ}30'42''$

Obs. ID	Sequence	Observation date	Exposure (ks)	Nominal roll (deg)	Pointing RA	Pointing Dec
3209	800209	2002-08-08	95.8	101.2	3:19:46.86	+41:31:51.3
4289	800209	2002-08-10	95.4	101.2	3:19:46.86	+41:31:51.3
6139	800397	2004-10-04	51.6	125.9	3:19:45.54	+41:31:33.9
4946	800397	2004-10-06	22.7	127.2	3:19:45.44	+41:31:33.2
4948	800398	2004-10-09	107.5	128.9	3:19:44.75	+41:31:40.1
4947	800397	2004-10-11	28.7	130.6	3:19:45.17	+41:31:31.3
4949	800398	2004-10-12	28.8	130.9	3:19:44.57	+41:31:38.7
4950	800399	2004-10-12	73.4	131.1	3:19:43.97	+41:31:46.1
4952	800400	2004-10-14	143.2	132.6	3:19:43.22	+41:31:52.2
4951	800399	2004-10-17	91.4	135.2	3:19:43.57	+41:31:42.6
4953	800400	2004-10-18	29.3	136.2	3:19:42.83	+41:31:48.5
6145	800397	2004-10-19	83.1	137.7	3:19:44.66	+41:31:26.7
6146	800398	2004-10-20	39.2	138.7	3:19:43.92	+41:31:32.7

**Table 1.** *Chandra* observations included in this analysis. The exposure given is the time remaining after filtering the lightcurve for flares. All observations were taken with the aimpoint on the ACIS-S3 CCD. All positions are in J2000 coordinates.

As the X-ray diffuse emission of the NGC 1275 is very strong, the source list may well include false detections in high background level regions. Therefore problematic sources embedded in such regions have been excluded in our analysis. Moreover, as mentioned above, we only included sources associated with the HVS.

We have detected 8 bright sources close to the nucleus of NGC 1275, located in the northern inner radio lobe of 3C 84. All of these source are embedded in the same region as the HVS (see Fig. 1). There are no sources associated with the southern lobe (Fig. 1), thus we assume these sources are associated with the HVS.

Fig. 4 (*left*) shows the smoothed ACIS-S3 image in the 0.3–7.0 keV band, including numbered labels of all the detected sources (*top*), centred on source labelled N3 (*centre*) and centred on source N5 (*bottom*).

All the point-like sources are listed in Table 2, showing their positions and count rates.

We have used archival *HST* observations of NGC 1275 in order to search for optical counterparts. The galaxy was imaged with the WFPC2 camera on *HST* using the F814W ( $\sim I$ , on 2001 November 6 with an exposure time of 1200 s) and F702W ( $\sim R$ , on 1994 March 31 with an exposure time of 140 s) broad-band filters. Several coincidences between X-ray sources and optical knots of emission (F814W) can be seen in Fig. 4 (*right*), showing the same regions as Fig. 4 (*left*).

The *HST* image shows many highly absorbed features. When we compare in detail, sources N7 and N8 are located in star forming regions, while N2 and N6 have a point-like counterpart. Sources N1, N3, N4 and N5 have no optical identification. Therefore, we

N	Position(J2000)	Count Rate (counts ks <sup>-1</sup> )
1....	03:19:48.736 +41:30:47.25	0.34±0.05
2....	03:19:48.166 +41:30:46.64	1.69±0.06
3....	03:19:48.090 +41:31:01.88	2.60±0.08
4....	03:19:47.994 +41:30:52.30	1.42±0.09
5....	03:19:47.925 +41:30:47.50	1.19±0.09
6....	03:19:47.602 +41:30:47.01	0.74±0.06
7....	03:19:47.422 +41:30:51.93	0.95±0.08
8....	03:19:47.214 +41:30:47.62	1.28±0.08

**Table 2.** Positions of sources detected near the NGC 1275 centre and displayed in Fig. 4 (column 2) and count rate in the energy range between 0.5–7.0 keV (column 3).

N	F <sub>X</sub> /F <sub>F814W</sub>	F <sub>X</sub> /F <sub>F702W</sub>	M <sub>F814W</sub>	M <sub>F702W</sub>
1....	> 26.5	> 16.2	>22.6	>22.1
2....	25.4	23.6	20.4	20.3
3....	>18800	...	>26.8	...
4....	>1081	>800	>24.5	>24.2
5....	>123	>60.6	>22.6	>21.9
6....	26.2	28.4	21.7	21.7
7....	76.7	51.4	22.3	21.9
8....	134	90.1	22.2	21.7

**Table 3.** Optical analysis. X-ray to optical ratios (columns 2 and 3) and magnitude determinations (columns 4 and 5) for the filters F814W and F702W, respectively, with the X-ray flux between 1.0–7.0 keV.

have found a possible correlation between compact X-ray sources and regions of vigorous star formation. The implications are discussed later.

In order to investigate the emission mechanism of these ULX, the X-ray to optical flux ratios have been computed between the F702W and F814W *HST* broad-bands and 1.0–7.0 keV X-ray band. Preliminary processing of the raw images including corrections for the flat fielding was done remotely at the *Space Telescope Science Institute* through the standard pipeline. For each frame, cosmic rays were removed by image combination, using the IMCOMBINE routine in IRAF. After cosmic ray removal, the frames were added using task WMOSAIC in STSDAS package. Photometric measurements were made with PHOT task, within the NOAO package. Finally the fluxes and magnitudes have been determined using the photometric zero-point information in the header of the calibrated image files.

These results are shown in Table 3, including the X-ray to optical flux ratios from the F814W and F702W broad-band filters, and the magnitude determinations from the same filters. In the cases where an optical counterpart has not been found (N1, N3, N4 and N5), the magnitudes and fluxes are just a lower limit.

### 3 SPECTRAL ANALYSIS

We extracted spectra for all the detected sources close to the HVS, using extraction regions defined to include as many of the source photons as possible, but at the same time minimizing contamination from nearby sources and background. The background region was

N	N <sub>H</sub> (10 <sup>21</sup> cm <sup>-2</sup> )	Γ	χ <sup>2</sup> /d.o.f.
1....	2.5 <sup>(a)</sup>	3.20 <sup>+0.23</sup> <sub>-0.37</sub>	112.90/101
2....	2.72 <sup>+1.43</sup> <sub>-0.87</sub>	1.78 <sup>+0.30</sup> <sub>-0.24</sub>	101.50/109
3....	2.49 <sup>+0.40</sup> <sub>-0.40</sub>	2.08 <sup>+0.09</sup> <sub>-0.09</sub>	153.86/142
4....	2.05 <sup>+0.91</sup> <sub>-0.96</sub>	2.29 <sup>+0.44</sup> <sub>-0.28</sub>	156.24/152
5....	2.64 <sup>+1.23</sup> <sub>-0.93</sub>	2.92 <sup>+1.44</sup> <sub>-0.36</sub>	124.09/139
6....	3.74 <sup>+1.57</sup> <sub>-1.39</sub>	3.51 <sup>+0.48</sup> <sub>-0.66</sub>	102.58/92
7....	4.03 <sup>+1.78</sup> <sub>-1.45</sub>	3.20 <sup>+1.39</sup> <sub>-0.48</sub>	133.69/135
8....	2.66 <sup>+1.00</sup> <sub>-0.91</sub>	2.13 <sup>+0.52</sup> <sub>-0.25</sub>	150.81/138

**Table 4.** Spectral fits. (a) The column density of source N1 has been fixed due to the low count rate.

N	F <sub>obs</sub> (0.5–7.0 keV) erg cm <sup>-2</sup> s <sup>-1</sup>	F <sub>corr</sub> (0.5–7.0 keV) erg cm <sup>-2</sup> s <sup>-1</sup>	log L <sub>X</sub> 0.5–7.0 keV
1....	2.09 × 10 <sup>-15</sup>	4.34 × 10 <sup>-15</sup>	39.51
2....	7.59 × 10 <sup>-15</sup>	9.97 × 10 <sup>-15</sup>	39.86
3....	1.64 × 10 <sup>-14</sup>	2.28 × 10 <sup>-14</sup>	40.22
4....	7.76 × 10 <sup>-15</sup>	1.10 × 10 <sup>-14</sup>	39.91
5....	5.36 × 10 <sup>-15</sup>	1.07 × 10 <sup>-14</sup>	39.90
6....	3.02 × 10 <sup>-15</sup>	9.23 × 10 <sup>-15</sup>	39.84
7....	4.28 × 10 <sup>-15</sup>	1.18 × 10 <sup>-14</sup>	39.95
8....	7.67 × 10 <sup>-15</sup>	1.16 × 10 <sup>-14</sup>	39.93

**Table 5.** Fluxes (observed and k-corrected) and luminosities assuming a cosmological model with H<sub>0</sub> = 70 km s<sup>-1</sup>Mpc<sup>-1</sup> and z=0.018.

either a source-free circular annulus or several circles surrounding each source, in order to take into account the spatial variations of the diffuse emission and to minimize effects related to the spatial variation of the CCD response.

For each source, we extracted spectra from each of the datasets. These spectra were summed to form a total spectrum for each source. Response and ancillary response files were created for each source in each of the observations using the CIAO MKACIS-RMF and MKWARF tools. The responses for a particular source were summed together, weighting according to the number of counts in each observation.

The spectra were fitted using XSPEC v.11.3.2. In order to use the χ<sup>2</sup> statistic, we grouped the data to include at least 20 counts per spectral bin, before background subtraction. In spectral fitting we excluded any events with energies above 7.0 keV or below 0.5 keV.

Table 4 summarizes our spectral results in terms of the absorbing column density and photon index.

The sources have been modelled with an absorbed power law slope with photon index between Γ = [1.78–5.56] and an equivalent column density of N<sub>H</sub> = [2.05 – 4.03] × 10<sup>21</sup> cm<sup>-2</sup>. In all the cases the single component power law give satisfactory fits. The column density of source N1 has been fixed due to the low count rate. The fitted N<sub>H</sub> values are consistent with the intrinsic absorption measured e.g. in the optical band; the value of A<sub>V</sub>=0.54 corresponds to N<sub>H</sub> ~ 1.1 × 10<sup>21</sup> cm<sup>-2</sup>, assuming A<sub>V</sub> = N<sub>H</sub> × 5.3 × 10<sup>-22</sup> for R<sub>V</sub> = 3.1 (Bohlin et al. 1978). This value should be a lower limit to the fitted N<sub>H</sub> value to be consistent, as is seen in Table 4.

As an example of our spectral fits, the brightest source, N3, has been fitted with a power-law with spectral index of 2.08 ± 0.09 and absorption of N<sub>H</sub> = 2.5 ± 0.4 × 10<sup>21</sup> cm<sup>-2</sup> (see Fig. 3).

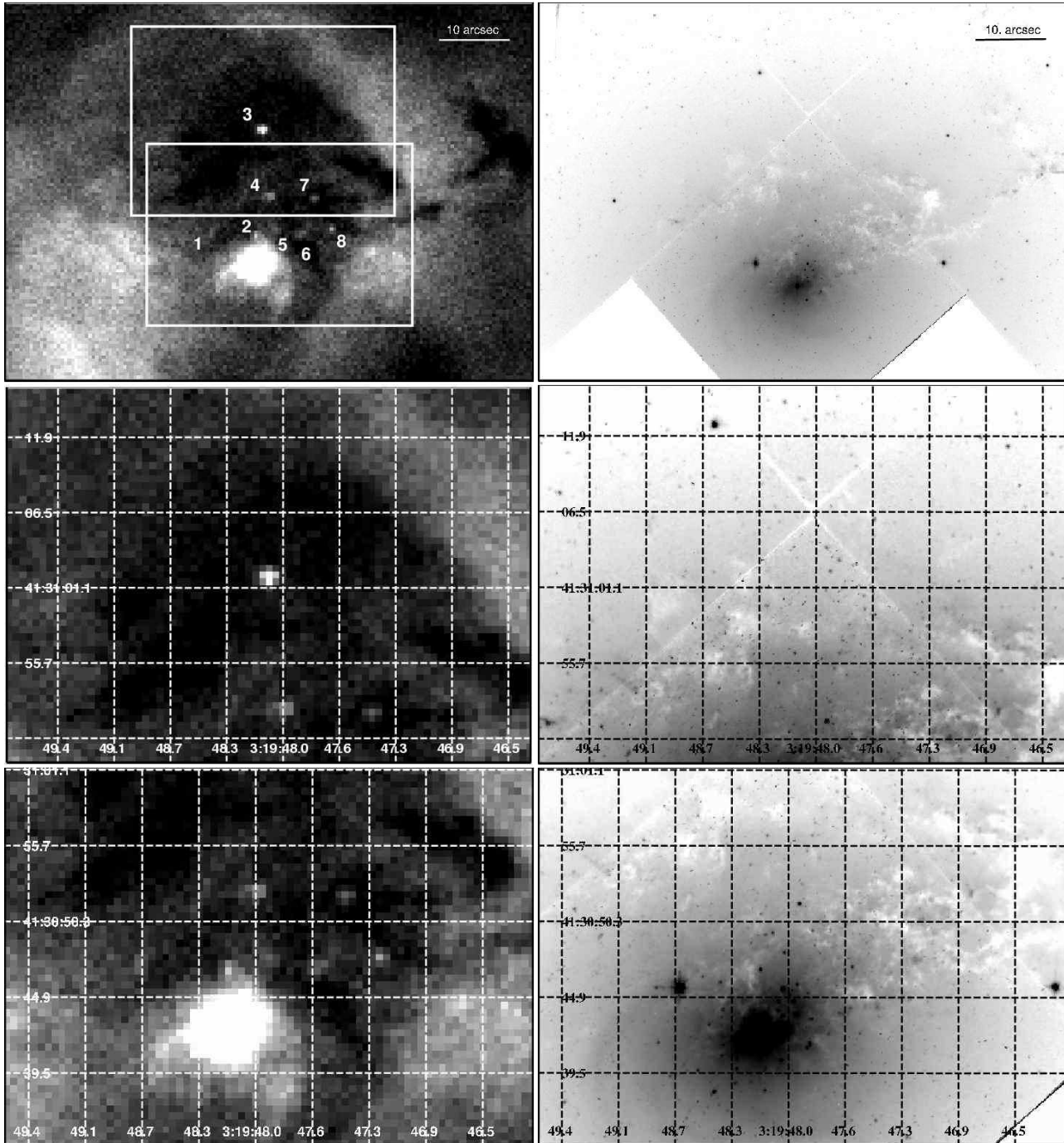


**Figure 4.** Top-left: Broadband (0.5–7.0 keV) X-ray smoothed image with sources labelled. Top-right: *HST*/WFPC2 F814W broadband image. Centre-left: Broadband (0.5–7.0 keV) X-ray smoothed image centred in source 3. Centre-right: *HST*/WFPC2 F814W broadband image centred in source 3. Bottom-left: Broadband (0.5–7.0 keV) X-ray smoothed image centred in source 5. Bottom-right: *HST*/WFPC2 F814W broadband image centred in source 5.

In Table 5 we list the 0.5–7 keV flux and (absorption corrected) luminosities of the individual sources based on the best-fit power law model.

The lower limit of the luminosity of point sources in the image, if at the distance of NGC 1275, is  $L_X(0.5 - 7.0 \text{ keV}) = 3.2 \times 10^{39} \text{ erg s}^{-1}$ , which is already well above the Eddington limit for a neutron star binary ( $L_X \sim 3 \times 10^{38} \text{ erg s}^{-1}$ ) and is also above the limit of canonical ULX, i.e.  $\geq 10^{39} \text{ erg s}^{-1}$ .

The brightest point source has a luminosity of  $L_X(0.5 - 7.0 \text{ keV}) = 1.67 \times 10^{40} \text{ erg s}^{-1}$ , and is one of the brightest individual sources found in a galaxy. A ULX source more luminous than the entire X-ray luminosity of a normal galaxy has been found in the Cartwheel system with a luminosity of at least  $L_X \sim 2 - 4 \times 10^{40} \text{ erg s}^{-1}$  (Gao et al. 2003; Wolter & Trinchieri 2004). They explain this luminosity with a high-mass X-ray binary source (HMXB). The high X-ray luminosity suggests either a single extremely bright source, or a very dense collection of several

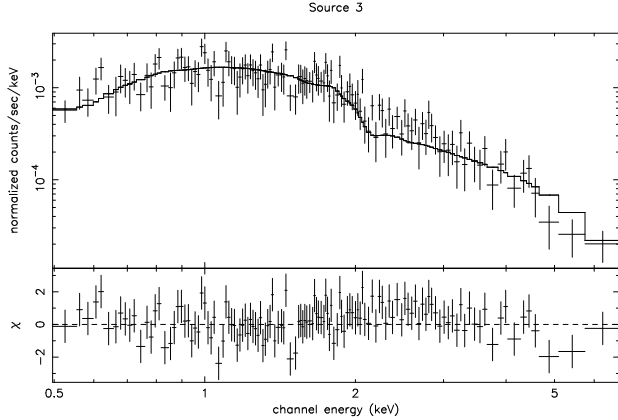


**Figure 3.** ACIS-S spectrum of source N3. The solid line corresponds with a power law model with a spectral index of  $\Gamma=2.08$  and absorption of  $N_{\text{H}} = 2.5 \times 10^{21} \text{ cm}^{-2}$ . The fit residuals are presented in the lower panel.

high  $L_{\text{X}}$  sources, which would be even more peculiar. Evidence of time variability might suggest that is a single high  $L_{\text{X}}$  source.

Time variability analysis has been performed. The observations span about two years. Two data files were observed on 2002 August 8 and 10, and the other eleven data files were observed from 2004 October 4 to 2004 October 20, giving an almost daily coverage. The exposure times are between 22 and 143 ks. The data characteristics allows us determine short variation in 16 days (second period) and long-term variability of 2 years. Because of the low count rates of the sources in NGC 1275 (see Table 2), it is very hard to search for short-term variability. We extracted light-curves, using DMEXTRACT CIAO task for the two brightest sources (N3 and N4) (net count rate greater than  $0.98 \text{ count s}^{-1}$ ) binned with bin sizes of 500, 1000, 2500 and 5000 s. In both cases the points were consistent with the respective mean values and variability has not been found. Furthermore, the mean values between 2002 and 2004 are the same, including errors bars. Therefore, evidence of time variability has not been found during the whole set of observations.

#### 4 DISCUSSION

*Chandra* has revealed significant populations of ULX in the interacting systems of the Antennae (NGC 4038/9; Zezas, Fabbiano & Murray 2002) and the Cartwheel ring galaxy (Gao et al. 2003; Wolter & Trinchieri 2004), where dramatic events have stimulated massive star formation. We have reported here on another example (Fig. 4 left) in the HVS of NGC 1275 which is interacting with the ICM of the Perseus cluster.

The sources are spatially associated with the distribution of absorbing clouds seen in soft X-ray (Fig. 2) and optical (Fig. 3) images. Two sources (N7 and N8) are directly linked with dust knots and another two (N2 and N6) have an optical point-like counterpart (Fig. 4 bottom). Similar correspondence have been found in the Cartwheel galaxy with the outer ring (Wolter & Trinchieri 2004) and in the Antennae galaxies with 39 X-ray sources within the WFPC2 field (Zezas et al. 2002). The optical brightness of the counterparts in the HVC are too high to be individual stars and so may be associated with young star clusters. Following the discussion of young star clusters in NCG 1275 given by Richer et al (1993), an object of magnitude 22 corresponds to a cluster mass of about  $10^6 M_{\odot}$  if its age is about  $10^7$  yr. The HVC system travels at least 30 kpc in  $10^7$  yr so if a strong interaction with the core of

the Perseus galaxy cluster has triggered star cluster formation in the HVC, then the clusters should have ages less than  $\sim 10^8$  yr.

Our interpretation of the spatial correspondence with star clusters is that the regions are especially active, indicating a real link between ULX and star-forming regions, and meaning they are young objects. However the optical limits on sources N3 and 4 rule out any association with massive clusters in those cases (the limit on the absolute magnitude is about  $-8$ ).

In M31 and the Milky Way (Grimm, Gilfanov & Sunyaev 2003), XRB have luminosities consistent with the Eddington limit of a  $\sim 2M_{\odot}$  accreting object. They produce luminosities  $\sim 3 \times 10^{38} \text{ erg s}^{-1}$ , about one order of magnitude below the limiting luminosity in our sample ( $3.2 \times 10^{39} \text{ erg s}^{-1}$ ). It is possible that our ULX consist of at least 15 (or 130, in the case of the brightest source found) ‘normal’ XRB clustered together, perhaps in a young star cluster. However in other objects we know that variability requires the presence of intrinsically luminous X-ray sources (e.g. M82; Griffiths et al. 2000, Kaaret et al. 2001). Alternative possibilities are that black hole sources, with masses in the range of galactic black hole binaries, are mildly beamed (Reynolds et al. 1999 and King et al. 2001). Spectral and timing features however rule out this possibility in some ULX (e.g. Strohmayer & Mushotzky 2003). We note that compact supernova remnants sometimes have ULX luminosities (e.g. Fabian & Terlevich 1998), but no recent supernovae have been reported for NGC 1275 (SN1968A was to the S of the HVS; Capetti 2002).

Finally, we recall the IMBH model which has spectral support from some sources (Miller et al 2004; the level of absorption in NGC 1275 is too high for any soft excess to be observed). They may form in dense star clusters.

Our optical studies have clearly shown that the ULX have very high X-Ray to optical flux ratios. X-ray selected AGN from the *Rosat all sky survey* tend to have  $\log(F_{\text{X}}/F_{\text{opt}}) \sim 1$ . Thus the ULX do not have the optical properties expected if their were simple extensions of AGN (IMBH, as low luminosity limit). However, low mass X-ray binaries in the Milky Way have  $F_{\text{X}}/F_{\text{opt}} \sim 100 - 10000$  (Mushotzky 2004).

The results found in our system indicate that we have a mixed group of objects (see Table 3). At least 4 out of 8 sources (N3, N4, N5 and N8) have high X-ray to optical flux ratios. At least 3 out of 8 (N1, N2 and N6) have lower X-ray to optical ratios, possibly because they lie in star clusters.

Our data are consistent with no significant variability, similar to the result obtained on NGC 3256 by Lira et al. (2002). Time variability is frequently observed in ULX (e.g. IC 342, Sugiho et al. 2001 or M51 X-1, Liu et al. 2002), arguing that most of them are single compact objects, rather than a sum of numerous lower luminosity objects in the same object. While most ULX vary, many show low amplitude variability on long time scales (e.g. the Antennae galaxies, Zezas et al. 2002), which is very different to galactic black holes. Portegies Zwart, Dewi & Maccarone (2004) find that a persistent bright ULX requires a doner star exceeding  $15 M_{\odot}$ . The search for characteristic frequencies is one of the most productive way of determining the nature of the ULX.

#### 5 CONCLUSIONS

We have described the detailed analysis of the spatial and spectral properties of the discrete X-ray sources detected with a deep *Chandra* ACIS-S observation around NGC 1275. Our results are summarized below:

(i) We have detected a total of 8 sources to the north of NGC 1275 nucleus.

(ii) The sources are spatially coincident with the High Velocity System and thus probably associated with it. They are therefore ULX.

(iii) Four of the sources have an optical counterpart in the I and R bands (from *HST* images); two of which are point-like sources and the other two are associated with star-forming regions.

(iv) In all the cases a single component power law gives satisfactory fits, with spectral index of  $\Gamma = [1.78-3.51]$  and an equivalent column density of  $N_{\text{H}} = [2.05 - 4.03] \times 10^{21} \text{ cm}^{-2}$ .

(v) The minimum luminosity is  $L_{\text{X}}(0.5 - 7.0 \text{ keV}) = 3.2 \times 10^{39} \text{ erg s}^{-1}$  (source N1), which is already above the limit of canonical ULX.

(vi) No variability was detected in the two brightest sources found.

Our results add to the growing evidence that some episodes of rapid star formation lead to the production of ULX. Young, massive, star clusters may be involved in some, but not all of the sources.

## ACKNOWLEDGEMENTS

OGM acknowledges the financial support by the Ministerio de Educacion y Ciencia through the program AYA2003-00128 and grant FPI BES-2004-5044. ACF thanks the Royal Society for support.

## REFERENCES

- Begelman M.C., 2002, *ApJ*, 568, L97  
 Bohlin R. C., Savage B. D., Drake J. F., 1978, *ApJ*, 224, 132  
 Boroson T. A., 1990, *ApJ*, 360, 465  
 Capetti, A., 2002, *ApJ*, 574, L25  
 Caulet A, Woodgate B E., Brown L. W., Gull T, R., Hintzen P, Lowenthal J. D., Oliverson R. J., Ziegler M. M., 1992, *ApJ*, 388, 301  
 Conselice C. J., Gallagher J. S., Wyse R. F., 2001, *AJ*, 122, 2281  
 Fabbiano G., White N.E., 2003, astro-ph/0307077  
 Fabbiano G., Zezas A., Murray S., 2001, *ApJ*, 554, 1035  
 Fabian A.C., Terlevich R., 1996, *MNRAS*, 280, L5  
 Gao Y., Wang Q. D., Appleton P. N., Lucas R. A., 2003, *ApJ*, 596, L171  
 Gebhardt K., Rich R.M., Ho L.C., *ApJ*, in press, astro-ph/0508251  
 Gillmon K., Sanders J. S., Fabian A. C., 2004, *MNRAS*, 348, 159  
 Griffiths R. E., Ptak A., Feigelson E. D., Garmire G., Townsley L., Brandt W. N., Sambruna R., Bregman J. N., 2000, *Science*, 290, 1325  
 Grimm H., Gilfanov M., Sunyaev R., 2003, *MNRAS*, 339, 793  
 Haschick A. D., Crane P. C., van der Hulst J., 1982, *ApJ*, 262, 81  
 Holtzman J. A., Faber S. M., Shaya E. J., Lauer T. R., Groth J., Hunter D. A., Baum W. A., Ewald S. P., Hester J. J., Light R. M., Lynds C. R., O'Neil E. J., Westphal J. A., 1992, *AJ*, 103, 691  
 Kaaret P., Prestwich A. H., Zezas A., Murray S. S., Kim D.-W., Kilgard R. E., Schlegel E. M., Ward, M. J., 2001, *MNRAS*, 321, L29  
 King A. R., Davies M. B., Ward M. J., Fabbiano G., Elvis, M., 2001, *ApJ*, 552, L109  
 Lira P., Ward M., Zezas A., Alonso-Herrero A., Ueno S., 2002, *MNRAS*, 330, 259  
 Liu J., Bregman J. N., Irwin J., Seitzer P., 2002, *ApJ*, 581, L93  
 Makishima K., Kubota A., Mizuno T., Ohnishi T., Tashiro, M., Aruga Y., Asai K., Dotani T., Mitsuda K., Ueda Y., Uno S., Yamaoka K., Ebisawa K., Kohmura Y., Okada K., 2000, *ApJ*, 535, 632  
 Miller J. M., Fabian A. C., Miller M. C., 2004, *ApJ*, 614, L117  
 Miller J.M., Colbert E., 2004, *IJ Mod. Phys.*, 13, 1  
 Minkowski R., 1955, *Carnegie Yearbook*, 54, 25

- Minkowski R., 1957, in Van de Hulst H.C., ed., *Proc. IAU Symp.* 4, Radio Astron. Cambridge Univ. Press, Cambridge, p. 107  
 Mushotzky R., 2004, *Prog. of Theo. Phys. Supplement*, 155, 27  
 Portegies Zwart S. F., McMillan S. L. W., 2002, *ApJ*, 576, 899  
 Portegies Zwart S. F., Dewi J., Maccarone T., 2004, *MNRAS*, 355, 413  
 Reynolds C. S., Henz S., Fabian A. C., Begelman M.C., 1999, *ApJ*, 521, 99  
 Richer, H.B., Crabtree, D.R., Fabian, A.C., Lin, D.N.C., 1993, *AJ*, 105, 877  
 Sarazin C. L., 1988, *X-Ray Emissions from Clusters of Galaxies*, Cambridge Univ. Press, Cambridge.  
 Sugiho M., Kotoku J., Makishima K., Kubota A., Mizuno T., Fukazawa Y., Tashiro M., 2001, *ApJ*, 561, L73  
 Strohmayer T.E., Mushotzky R. F., 2003, *ApJ*, 586, L61  
 Wolter A., Trinchieri G., 2004, *A&A*, 426, 787  
 Zezas A., Fabbiano G., 2002, *ApJ*, 577, 726  
 Zezas A., Fabbiano G., Rots A. H., Murray S. S., 2002, *ApJ Supplement*, 142, 239